Bone 157 (2022) 116327

Contents lists available at ScienceDirect

Bone

journal homepage: www.elsevier.com/locate/bone

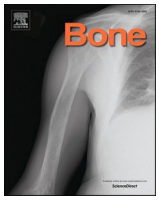

Full Length Article

# Perilacunar bone tissue exhibits sub-micrometer modulus gradation which depends on the recency of osteocyte bone formation in both young adult and early-old-age female C57Bl/6 mice

Caleb J. Rux [a,b], Ghazal Vahidi [a], Amir Darabi [a], Lewis M. Cox [a], Chelsea M. Heveran [a,*]

[a] Department of Mechanical & Industrial Engineering, Montana State University, United States of America
[b] UC Berkeley-UCSF Graduate Program in Bioengineering, United States of America

ARTICLE INFO

*Keywords:*
Atomic force microscopy
Osteocyte
Lacunae
Lacunar-canalicular remodeling
Aging
Bone

ABSTRACT

Osteocytes resorb and replace bone local to the lacunar-canalicular system (LCS). However, whether osteocyte remodeling impacts bone quality adjacent to the LCS is not understood. Further, while aging is well-established to decrease osteocyte viability and truncate LCS geometry, it is unclear if aging also decreases perilacunar bone quality. To address these questions, we employed atomic force microscopy (AFM) to generate nanoscale-resolution modulus maps for cortical femur osteocyte lacunae from young (5-month) and early-old-age (22-month) female C57Bl/6 mice. AFM-mapped lacunae were also imaged with confocal laser scanning microscopy to determine which osteocytes recently deposited bone as determined by the presence of fluorochrome labels administered 2d and 8d before euthanasia. Modulus gradation with distance from the lacunar wall was compared for labeled (i.e., bone forming) and non-labeled lacunae in both young and aged mice. All mapped lacunae showed sub-microscale modulus gradation, with peak modulus values 200–400 nm from the lacunar wall. Perilacunar modulus gradations depended on the recency of osteocyte bone formation (i.e., the presence of labels). For both ages, 2d-labeled perilacunar bone had lower peak and bulk modulus compared to non-labeled perilacunar bone. Lacunar length reduced with age, but lacunar shape and size were not strong predictors of modulus gradation. Our findings demonstrate for the first time that osteocyte perilacunar remodeling impacts bone tissue modulus, one contributor to bone quality. Given the immense scale of the LCS, differences in perilacunar modulus resulting from osteocyte remodeling activity may affect the quality of a substantial amount of bone tissue.

## 1. Introduction

Osteocytes, the most common cells in bone, live in a dense interconnected network of micrometer-scale voids in mineralized bone tissue (lacunae) connected by sub-micrometer-radius channels (canaliculi) [1–7]. The lacunar-canalicular system (LCS) has an estimated 215 $m^2$ surface area in the human skeleton [7] and its trillions of connections allow for osteocytes to communicate within the skeletal network as well as to the kidneys, parathyroid, vasculature, and muscle [5,8,9]. Osteocytes can modulate the size of the LCS through either resorbing bone [10–14] or replacing new osteoid [1,11,15–21] in a process termed LCS remodeling. This process contributes to systemic calcium homeostasis, as demonstrated by expanding lacunae and canaliculi in lactation and recovery after weaning [11,15,22]. It is not yet understood if LCS remodeling also contributes to the maintenance of bone quality. This question is of importance because LCS geometries truncate in aging [2,21,23–30], which suggests that aging alters LCS remodeling activity.

Prior work suggests that LCS remodeling has the potential to reduce bone quality. In DMP1 – conditional TGFβ receptor deletion [31] and global knockout of MMP13 [32], both phenotypes demonstrate reduced LCS remodeling activity together with reduced notched fracture toughness. However, it is not clear why bone with less LCS remodeling has lower bone fracture resistance. It is possible that morphological changes to the LCS affect the tendencies of cracks to initiate and propagate. On the other hand, LCS remodeling could directly benefit bone quality. Improvements in bone quality with LCS remodeling could result

* Corresponding author. Department of Mechanical & Industrial Engineering, Montana State University, P.O. Box 173800, Bozeman, MT 59717, United States of America.
*E-mail address:* chelsea.heveran@montana.edu (C.M. Heveran).

https://doi.org/10.1016/j.bone.2022.116327
Received 22 October 2021; Received in revised form 19 December 2021; Accepted 7 January 2022
Available online 11 January 2022

from a decrease in tissue maturity (e.g., decreased mineralization and modulus) in the vicinity of lacunae and canaliculi, since overly mature tissue is less able to engage intrinsic toughening mechanisms such as fibrillar sliding [33,34]. However, it has not been evaluated whether bone material properties near the LCS are influenced by the remodeling activity of the osteocyte.

It is possible to evaluate bone modulus gradations near bone-forming and non-bone-forming osteocytes by using fluorochrome labeling and high-resolution material property mapping. Fluorochrome labels are small enough to travel through the LCS and are observed to label lacunae [35–42]. While they may also label canaliculi, most confocal techniques lack the appropriate resolution to discern these smaller features. Bone quality adjacent to lacunae has usually been evaluated with conventional microscale-resolution bone quality characterization tools (i.e., Raman spectroscopy, nanoindentation, quantitative backscattered scanning electron microscopy), but these techniques fail to identify material property variation near lacunae outside of extreme phenotypes [6,15,34,43–48]. The lack of detection of material property variation near lacunae is likely a reflection of the limited resolution of these tools, since line profiles collected through synchrotron-based techniques with nanoscale resolution demonstrate mass gradation near lacunae and canaliculi on the scale of hundreds of nanometers away from LCS walls [1,49]. To date, perilacunar bone modulus has been mapped with AFM [6] but the spatial gradation of modulus has not been quantified. Furthermore, the gradation in perilacunar bone modulus has not been compared for bone-forming and non-bone-forming osteocytes and has not been compared for young and aged bone.

Atomic force microscopy (AFM) is well-suited for mapping bone modulus near bone-forming and non-bone-forming osteocytes. AFM can quantitatively assess modulus on the order of 10s of nanometers using fast force mapping techniques. AFM has been used to demonstrate that modulus is heterogeneous near lacunae and canaliculi in 4-month female Wistar rats, although this study did not identify whether characteristic modulus gradients exist with respect to distance from the LCS, nor whether these gradients depend on osteocyte bone formation or aging [6]. Several challenges exist in analyzing 2D perilacunar modulus maps, including reliably defining and smoothing the lacunar edge for a variety of lacunar shapes and sizes, sequentially expanding the lacunar edge by a given step size to create analysis regions (e.g., pixels with set range of distances from the lacunar wall), and determining appropriate step sizes for resolving modulus gradation with distance from the lacunar wall. Thus, we first sought to generate an analytic approach to analyzing 2D perilacunar modulus maps for the purpose of characterizing modulus gradation and comparing these gradations between bone-forming and non-bone-forming osteocytes at two ages.

The purposes of this study were to (1) develop an approach to analyze AFM-generated modulus maps of perilacunar bone for 2D spatial gradation, (2) determine whether labeled lacunae have different perilacunar modulus gradation than non-labeled lacunae, and (3) estimate whether aging impacts perilacunar modulus gradation. To investigate our research question, we utilized skeletally-mature young adult (5-month) and early-old-age (22-month) female C57Bl/6 mice, since this mouse model and age range produce marked changes in LCS morphology [20]. We hypothesized that lacunae would demonstrate modulus gradation in agreement with mass gradation reported with high-resolution techniques, that labeled lacunae would have lower moduli than non-labeled lacunae, and that aging would decrease the size of the region of lower-modulus bone near lacunae.

## 2. Materials and methods

### 2.1. Animal models

This investigation was conducted in two studies. The first study, in which methods were developed for AFM perilacunar bone modulus analysis, a 7-month-old female C57Bl/6 mouse was obtained from a live animal colony (group housed, 3 mice per cage, standard rodent chow and water provided ad libitum) at Montana State University. This mouse was euthanized via $CO_2$ inhalation. The second study, which evaluated the effects of age and label on perilacunar modulus gradation, included 5-month ($n = 5$) and 22-month-old (n = 5) female C57Bl/6 mice from Charles River Laboratory. These mice were administered calcein (20 mg/kg) and alizarin (30 mg/kg) labels via intraperitoneal injection 8d and 2d before euthanasia, respectively. An additional $n = 3$ mice per age were studied with label order reversed (e.g., alizarin administered at 8d, calcein administered at 2d). Mice were group housed (2–5 per cage), fed low fat diet (Research Diets D12450H; 10% kcal from fat) ad libitum for 8 weeks prior to euthanasia as controls for another study, provided water ad libitum, and euthanized via isoflurane inhalation. All animal procedures were approved by the Montana State University Institutional Animal Care and Use Committee.

### 2.2. Sample preparation

Left femurs were harvested and fresh frozen at −20 °C immediately after euthanasia. Femurs were gently thawed and tested to failure in three-point bending (results reported in a separate study). The distal halves of the femurs were histologically dehydrated in a graded ethanol series and embedded in poly(methyl) methacrylate (PMMA). Embedded distal femurs were sectioned at the midshaft using a low-speed diamond saw (Isomet, Buehler, Lake Bluff, IL) to obtain a transverse section with a 5 mm thickness. Then, cortical surfaces were polished with 600 and 1200 grits of wet silicon carbide papers (Buehler, Lake Bluff, IL), followed by fine polishing with Rayon fine cloths and different grades of alumina pastes (9, 5, 3, 1, 0.5, 0.3, and 0.05 μm) to achieve a mirror-like finish. Between polishing steps, sections were sonicated in tap water to remove any remaining particles. Embedded femur sections were mounted on a metal disk using epoxy (MasterBond EP29, Hackensack, NJ). A glass slide of the same 5 mm height was mounted next to the embedded femur section to be used for tip radius calibration.

An additional femur from a C57Bl/6 female 5-month-old mouse was harvested for a preliminary comparison of the effects of bone tissue hydration on perilacunar bone modulus. This mouse also received fluorochrome bone labels at 8d and 2d before euthanasia. The femur was not subjected to mechanical testing. The femur was air dried after tissue harvest, embedded in non-infiltrating epoxy (Buehler Epoxicure 2) and sectioned and polished consistent with the methods described for the PMMA-embedded specimens. The femur was never exposed to ethanol. The sample was rehydrated via immersion in tap water 10 min before AFM testing. The sample surface was wicked dry with a KimWipe before AFM testing.

### 2.3. AFM mapping

Atomic force microscopy (AFM) analyses were performed with an Asylum Research Cypher S force microscopy system with an etched silicon tip (RTESPA-525, 200 N/m spring constant, Bruker AFM Probes, Camarillo, CA). AFM was operated in two different modes: AC tapping mode (for topography scans) and fast force mapping (for modulus maps). Using AC tapping mode, the cantilever was driven at a constant amplitude at its resonance frequency and scanned across the surface to measure topography of the bone samples and to locate lacunae. Fast force mapping generated an array of local force-distance curves, obtained at high speed with nanometer spatial resolution, and was used to characterize modulus profiles around lacunae. Tip parameters were calibrated and resulting force curves were fit to a Hertzian contact model to calculate the contact modulus of the material (Fig. S5) [50]. First, calibration of a cantilever spring constant was obtained via thermal tune. Next, a force-distance curve was performed on a silicon wafer (Silicon Inc., Boise, ID) to calculate optical lever sensitivity. Once these values were obtained, tip radius was calibrated by first acquiring a fast force map (320 × 320-pixel map) of a glass surface with known modulus

(72 GPa, Fisherbrand, Pittsburgh, PA) then identifying the tip radius value needed to generate agreement of the Hertz model with the glass calibration surface.

For each bone, lacunae were randomly selected from the anterior side of the midshaft cortical cross-section. Selected lacunae were at least 20 μm away from bone endocortical and periosteal surfaces. A topographical lacunar map was first generated using AC mode, then fast force mapping generated a 512 × 512-pixel (12 × 12 μm map size at scan rate of 300 Hz) map of a lacuna with a ~ 20 nm resolution. A threshold of 500 nN was found to provide sufficient signal to noise ratio in the force curves and good agreement with the Hertzian contact models. While force curves represent an intermittent contact, rather than continuous contact technique, measurements of modulus must still account for potential tip wear. Tip radius was calibrated both before and after every fast force map of bone tissue was obtained, and the mean value of tip radius input into the Hertz model for modulus calculations. Tip radii were kept between 10 nm (pristine) and 20 nm at the start of the scan, as these values are consistent with typical tip wear in literature and are smaller than the resolution of acquired modulus maps [51,52]. The average change in tip radius was 1.06 nm per full scan, corresponding to approximately 5% drift in modulus for all samples. For reliability, we considered larger values of tip radius (i.e., > 20 nm) to violate the desired resolution and to have the potential for tip fracture or contamination and thus associated data were not considered. In our MATLAB-based segmenting and thresholding procedure, we excluded measurements <5 GPa since these values would be indistinguishable from PMMA, and a very small number of measurements >90 GPa as these values are most likely a result of indenting alumina beads embedded in the sample during polishing.

Six additional lacunae were mapped for a semi-hydrated femur (see Section 2.2) to estimate the effects of hydration on perilacunar modulus gradation. These lacunae were also located in the anterior quadrant, at least 30 μm away from periosteal or endocortical surfaces. AFM maps were obtained and analyzed as described for PMMA-embedded sections, with the exception that moduli values <5 GPa were not excluded, since there was not a plastic phase within the mapped area. AFM indentation extension curves did not show evidence of snap-on and thus the Hertz model was used for modulus calculations (Fig. S5).

### 2.4. Importing data and identifying the lacunar edge

Initially, square maps (equal number of x and y pixels) are imported to MATLAB as .csv files (Fig. 1a). The lacunar edge is defined for each map and points within the lacuna are masked out. Because dendrites extend from the lacunar wall, erosion is necessary to define a close-fitting lacunar edge. Erosion is performed based on a diamond-shaped element with size specified by the user (i.e., larger elements yield more aggressive erosion). The results of this step are shown in Fig. S1. This step creates an array of points that describes the lacunar boundary. This process is repeated to create an over-eroded boundary. This over-eroded boundary will be utilized later in the code to create sequential boundaries. An over-eroded boundary is required due to an inherent dilation when using a smoothing function later in the code.

### 2.5. Map and edge rotation

Next, maps are rotated about the lacunar centroid so that the ellipsoidal long axis of the lacuna is vertical. This step reduces distortion of sequential boundaries during dilation steps later in the code.

### 2.6. Creation of sequential boundaries

The lacunar edge boundary created from the over-erosion step will be used to create sequential boundaries (e.g., separated by a specified distance) surrounding the lacuna. User inputs include the number of desired dilations (e.g., number of sequential regions of interest with increasing distance from the lacunar wall), the distance between each boundary, and the map dimensions. The results of this step are

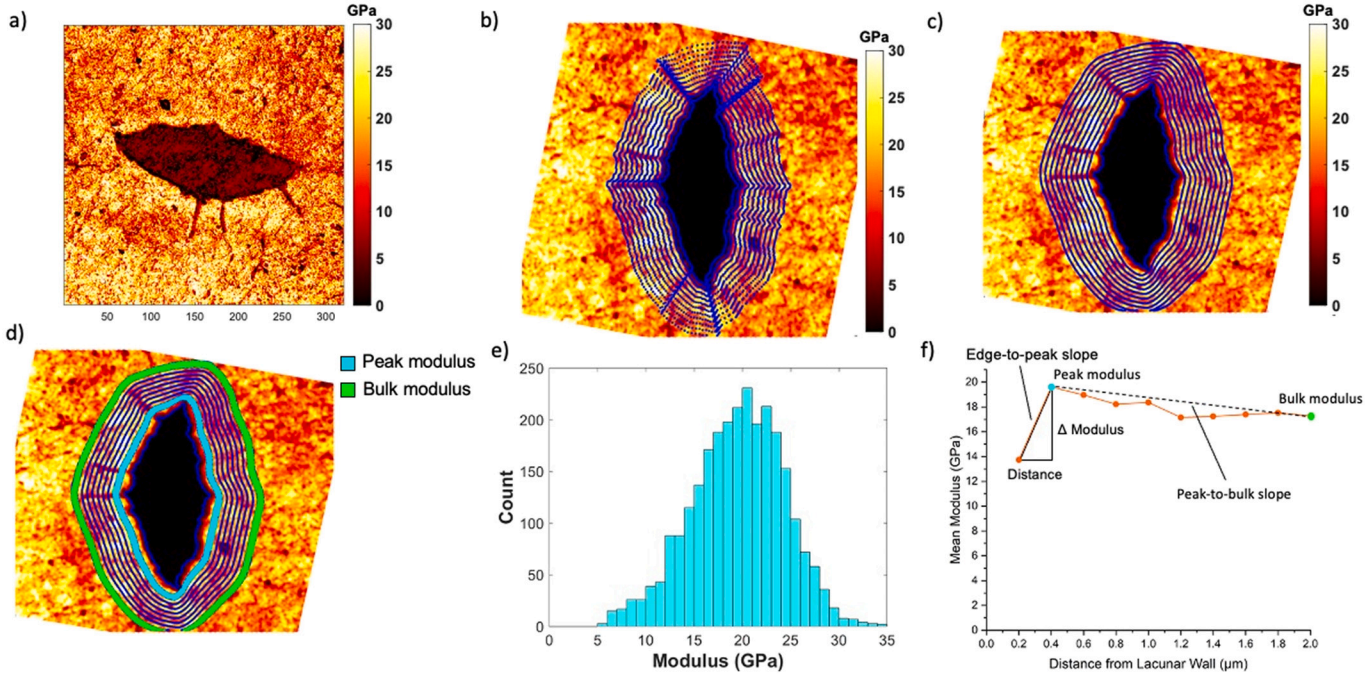


**Fig. 1.** a) An AFM modulus map for osteocyte perilacunar bone tissue. b) Raw modulus maps are processed through masking, rotation, and dilation steps. Sequential concentric rings are assigned for analysis. In this image, concentric rings are distanced by 0.2 μm. c) A convolution operation smooths boundaries to identify the lacunar wall. d-e) All pixels for an individual concentric ring, such as shown in cyan, are used to construct a histogram (bin size 1 GPa) of moduli. f) The modulus versus distance gradation profile corresponding to mean modulus values found within sequential concentric ring regions (cyan indicating the region that contains the peak mean modulus, green indicating the region that contains the bulk mean modulus value). (For interpretation of the references to colour in this figure legend, the reader is referred to the web version of this article.)

'unsmoothed' boundaries, as shown in Fig. 1b.

### 2.7. Smoothing of sequential boundaries

The sequential boundaries are then smoothed via a convolution matrix [53]. This achieves a boundary that closely matches lacunar geometry but removes more harsh edges and features that need not be considered. However, this step inherently dilates the lacunar edge somewhat, hence over-erosion is necessary in pre-processing (see Section 2.4). The results of the smoothing are shown in Fig. 1c.

### 2.8. Binning and analyzing points between concentric boundaries

Next, points within each two sequential boundaries are binned (Fig. 1d). The x-y position of each pixel is matched with a corresponding modulus. Lastly, a histogram is created for each region using a range of 1 GPa for histogram bin sizes (for example, if the range of the points within a certain region is 5.7 to 34.2 GPa there would be a bin for 5–6, 6–7, etc. up to 34–35) (Fig. 1e). Several statistical measurements are made for each concentric region, including mean, median, standard deviation, range, and full width at half maximum.

### 2.9. Analysis of modulus versus distance from the lacunar wall

Using measures calculated from histograms, modulus versus distance profiles were generated (Fig. 1f). From these profiles, measures included the peak modulus (greatest mean modulus of all concentric regions versus distance from the lacunar wall), the bulk modulus (the mean modulus of the last concentric ring, 1.8–2 μm), the difference between the peak and bulk measures, the edge-to-peak and peak-to-bulk slopes (GPa/μm), and perilacunar area before peak modulus. Additionally, slopes were also calculated after normalizing to the peak modulus of a given map. Peak to bulk difference and slopes were also calculated for standard deviations.

### 2.10. Confocal laser scanning microscopy imaging

Samples were imaged using an upright confocal microscope (Leica SP3,) with the following parameters: 40× water immersion lens, laser wavelength excitation of 488 nm (emission length 502–540) for calcein labels and 561 and 633 nm (emission length 580–645) for alizarin labels, pinhole set at 1 Airy unit, 1024 × 1024 resolution with a 600 Hz speed, and laser intensity set at 50% of the full power. The gain and offset were chosen such that in the images acquired the lacunae and their perilacunar remodeling were visible with minimum amount of noise. *Z*-stacks of images were acquired from the surface through the maximum depth where signal was observable, approximately 30 μm. The spacing between each slice was 0.8 μm. A composite image was formed by overlaying all slices (Imaris 9.3). Determination of whether a lacuna was labeled or not was made by evaluating composite images and then, in the case of potential non-labeled lacunae, checking each slice to confirm. All lacunae included in the study analysis (i.e., mapped with AFM and determined to be labeled or not labeled) were observable on the surface.

### 2.11. Data analysis

Mixed-model ANOVA evaluated the impact of the fixed effects of label (labeled vs no label) and age (5-month vs 22-month) and the random effect of individual mouse on measures pertaining to modulus variation near lacunae (e.g., peak modulus, bulk modulus, etc). Residuals for all models were checked for normality and equal variance. The dependent variable was natural log transformed, if necessary, to satisfy these assumptions. Significance was defined a priori as $p < 0.05$. In the case of a significant interaction between age and label, post-hoc tests were adjusted for family-wise error with the Bonferroni procedure (i.e., 2 comparisons: label vs non-labeled at each age; critical α adjusted to $p < 0.025$). All analyses were performed using Minitab v.19.

## 3. Results

We first developed AFM mapping and analysis techniques in order to determine whether perilacunar modulus demonstrates gradation with respect to distance from the lacunar wall and at what resolution this gradation is apparent. We then used these mapping and analysis parameters to investigate the influence of osteocyte bone formation activity on perilacunar modulus in skeletally-mature (5-month) and early-old-age (22-month) female C57Bl/6 mice.

### 3.1. Perilacunar bone tissue has sub-micrometer-scale modulus gradation

Atomic force microscopy fast force mapping demonstrates that bone modulus has sub-micrometer-scale gradation adjacent to osteocyte lacunae in cortical bone of the murine femur (Fig. 1a). To assess the effect of distance from the lacunar wall on modulus, we initially obtained eight maps from one 7-month female C57Bl/6 mouse. For each map, we binned pixels within regions of three different step sizes, 0.2, 0.5, and 1 μm, extending outward to 2 μm from the lacunar wall. The smallest step size, 0.2 μm, was selected because this distance is greater than the smallest lacunar spatial features but does not reduce the number of pixels per ring to such a low level as to impede interpretation of histograms. Further, gradations in mass density from synchrotron line profiles occur at a similar length scale [49]. We also studied 0.5 μm and 1 μm step sizes (i.e., averaging over all pixel modulus values within concentric rings of this width), since these resolutions are close to those of other common bone quality measurement techniques (e.g., Raman spectroscopy, backscattered scanning electron microscopy, nanoindentation). At each distance, a mean and a standard deviation were calculated from a histogram of all pixels within the region (Fig. 1).

Analysis of all maps at each of the three step sizes demonstrates that step size influences the ability to discern modulus gradation (Fig. 2a). At a step size of 0.2 μm, the modulus rose to a peak at 0.2–0.4 μm from the lacunar wall and then declined towards a bulk bone (i.e., 2 μm from the lacunar wall). These gradations were apparent in both raw data and data normalized to a peak value per lacunar map. The larger step sizes of 0.5 μm and 1 μm failed to capture the rise to a peak and decline to bulk seen in mean modulus values when using a finer 0.2 μm step size (Fig. 2a). Standard deviation was also evaluated at each step size. Using a 0.2 μm step size, standard deviation was found to be greatest close to the lacunar wall and declined within 0.4–0.6 μm to stable values (Fig. 2b). However, standard deviation was less sensitive to step size. All three step sizes detected a decrease in standard deviation with distance from the lacunar wall, although the resolution of this effect improves with finer step size. Modulus versus distance profiles for all eight lacunae mapped in this first study are shown in Figs. 3 and 4.

### 3.2. Bone-forming osteocytes have distinct perilacunar modulus gradation compared with non-bone-forming osteocytes

We first utilized confocal laser scanning microscopy (CLSM) to investigate whether labels administered 2 days and 8 days before euthanasia would be observed for 5-month- and 22-month-old mice. Calcein and alizarin labels were both abundantly observed for both ages of mice when administered 2 days before euthanasia (Fig. S2). By contrast, labels from calcein or alizarin administered at 8 days before euthanasia were infrequently observed, precluding comparison of perilacunar properties from different labeling dates. While future work would benefit from a closer labeling interval, our findings nonetheless suggest that osteocytes frequently deposit new osteoid and that this bone tissue undergoes frequent turnover.

We then evaluated whether osteocyte remodeling affects perilacunar

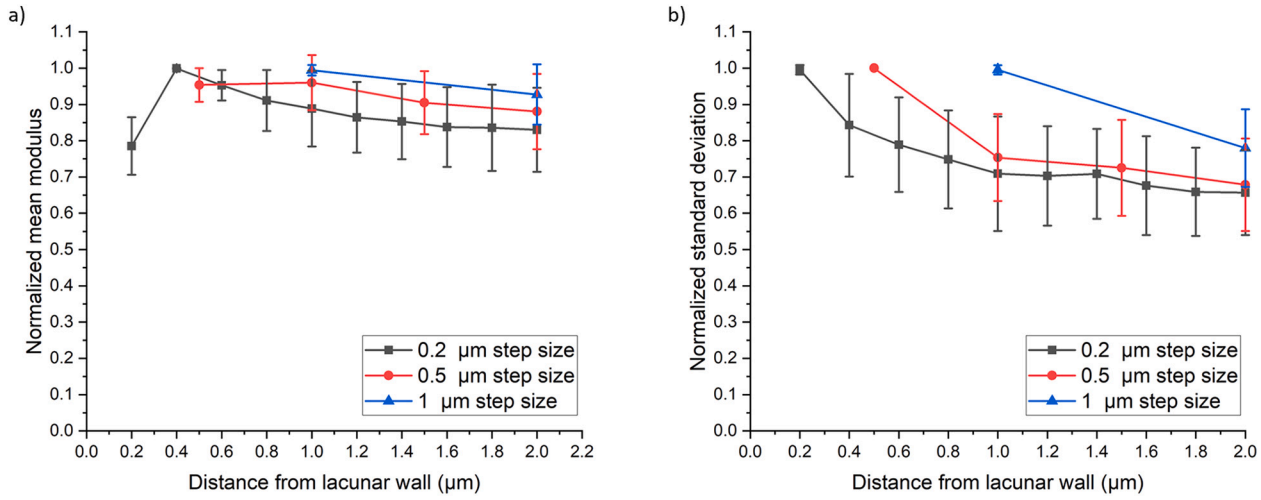


**Fig. 2.** a) Normalized mean moduli versus distance from the lacunar wall is plotted with data from 0.2, 0.5, and 1 μm step sizes extending to 2 μm from the lacunar edge. The distance from the lacunar wall indicates the outer distance of a bin (e.g., 0.4 μm means 0.2–0.4 μm). Error bars represent one standard deviation. b) Normalized standard deviations versus distance from the lacunar wall is plotted with data from 0.2, 0.5, and 1 μm step sizes extending to 2 μm from the lacunar edge. Error bars represent one standard deviation. Plots created from eight AFM maps obtained from lacunae from one 7-month female C57Bl/6 mouse.

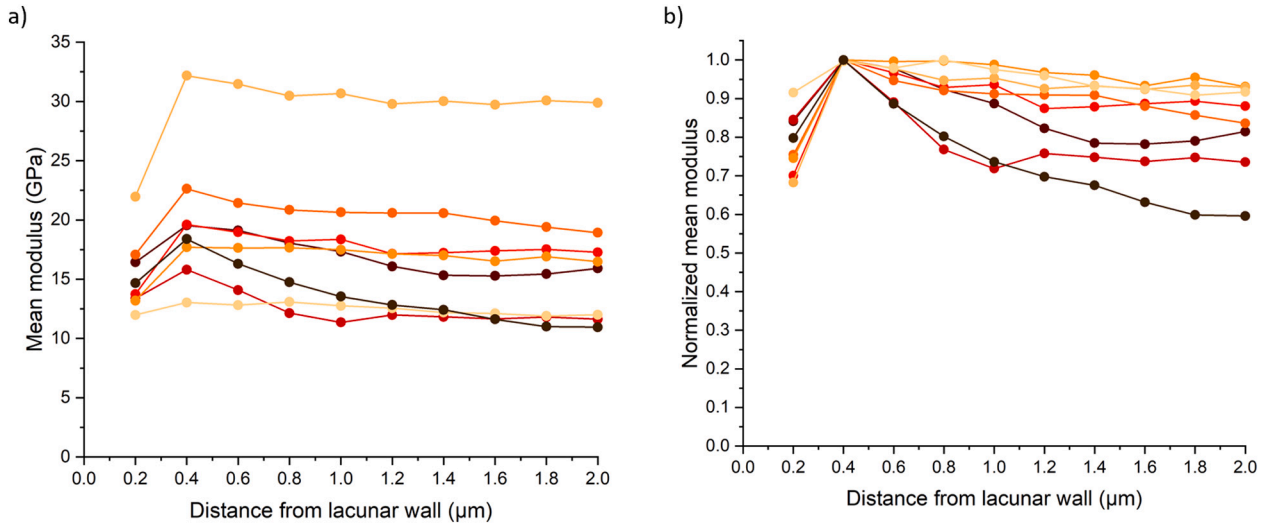


**Fig. 3.** a) Mean modulus for each concentric ring plotted against distance from the lacunar wall. The distance from the lacunar wall indicates the outer distance of a bin (e.g., 0.4 μm indicates the 0.2–0.4 μm bin). Connected dots each represent individual osteocyte lacuna map. b) Normalized mean modulus for each concentric ring plotted against distance from the lacunar wall. Mean modulus values were normalized against the peak mean modulus value for a given map. Plots created from eight AFM maps obtained from lacunae from one 7-month female C57Bl/6 mouse.

bone tissue modulus gradation (Figs. 5 and 6). Of the lacunae randomly selected for AFM mapping, 60% were labeled with alizarin (administered 2 days before euthanasia) for both 5-month and 22-month mice (5 lacunae/mouse, 5 mice/age, $N = 50$ lacunae). None of the mapped lacunae were labeled with calcein (administered 8 days before euthanasia). Mixed model ANOVA showed that labeled lacunae had lower peak modulus (−11.72%, $p < 0.05$) and bulk modulus (−10.06%, $p < 0.05$) (Table 1). There were no interactions between label and age for these measures. Of note, several labeled lacunae had much greater distance to the peak mean modulus. However, on average, the distance to peak mean did not differ between labeled and non-labeled lacunae. Labeled lacunae also had decreased peak standard deviation (−11.06%, $p < 0.05$) and bulk standard deviation (−12.61%, $p < 0.05$).

The presence of fluorochrome labels did not significantly affect other measures of modulus gradation, including slope of the lacunar edge to peak modulus and the slope from the peak modulus to bulk modulus (Table 1). Measures of lacuna size, including area, minor and major axis length, and sphericity (minor / major axes) were not different between labeled and non-labeled lacunae. Additionally, there were no significant interactions with labels and aging for these measures.

### 3.3. *Age affects some aspects of lacunar size and perilacunar modulus gradation*

The lacunar major axis was smaller for 22-month compared with 5-month mice (−11.93%, $p < 0.05$), although area and minor axes were not changed (we note that major and minor axis lengths were determined through obtaining an elliptical fit for each lacuna, while area was determined through the number of pixels thresholded out by the MATLAB image processing code). The mean slope peak-to-bulk was significantly impacted by age; 22-month mice showed a more gradual decrease in mean modulus from peak mean to bulk bone mean (−30.05%, $p < 0.05$, Table 1). There was a significant interaction between age and label for the bulk standard deviation normalized to the peak ($p < 0.05$). This

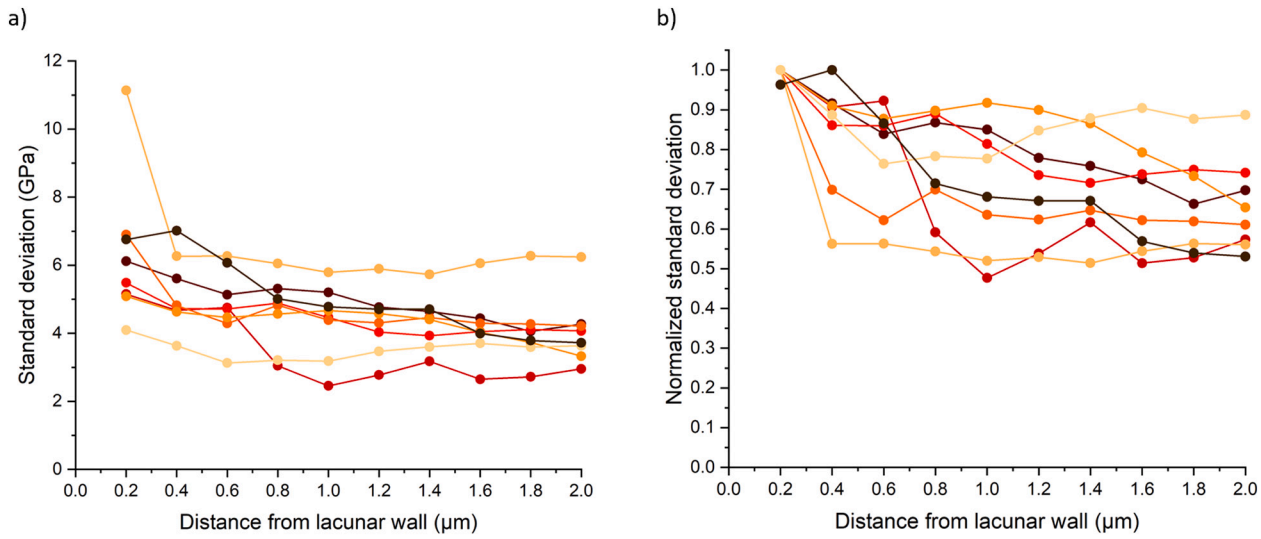


**Fig. 4.** a) Mean standard deviation for each concentric ring plotted against distance from the lacunar wall. The distance from the lacunar wall indicates the outer distance of a bin (e.g., 0.4 μm means 0.2–0.4 μm). Connected dots each represent individual osteocyte lacuna map. b) Normalized standard deviations for each concentric ring plotted against distance from the lacunar wall. Standard deviation values were normalized against the peak standard deviation value for a given map. Plots created from eight AFM maps obtained from lacunae from one 7-month female C57Bl/6 mouse.

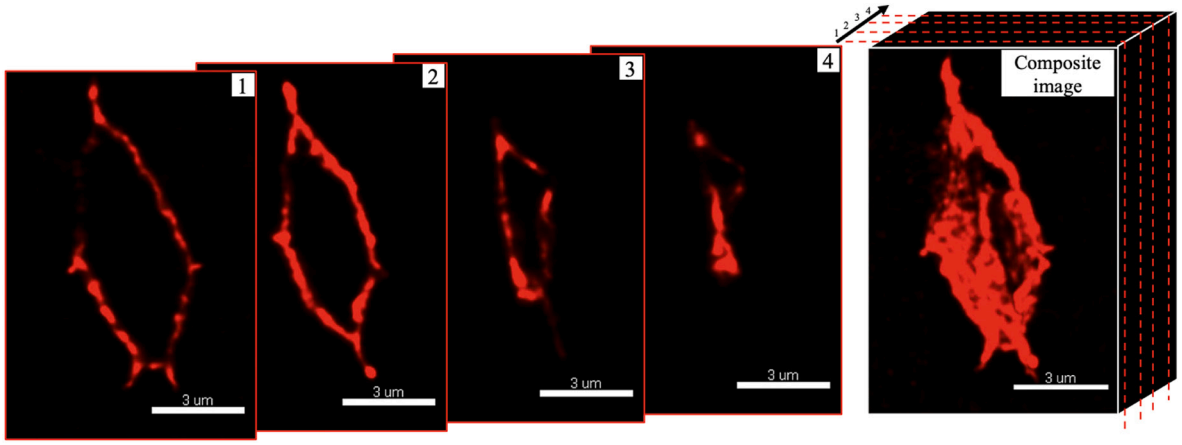


**Fig. 5.** Representative labeled lacuna from confocal microscopy. The composite image was generated from overlaying all slices for the *Z*-stack. Image 1 demonstrates labeling near the lacuna surface, while slices 2–4 show the progression of labeling with depth.

measure evaluates the difference in heterogeneity of bulk bone compared to near the lacunar edge (typically where the maximum standard deviation occurs). This interaction is driven by increased normalized standard deviation for labeled compared with non-labeled lacunae for young mice. However, the *p*-value (+13.35%, $p = 0.040$) is not small enough to be considered a significant difference given our Bonferroni correction for family-wise error. Importantly, several measures (e.g., lacunar sphericity, $p = 0.081$; modulus slope from edge:peak, $p = 0.070$) had the potential to be underpowered for the effect of age given our small sample size of $n = 5$ mice / age.

### 3.4. Lacunar size and shape do not strongly correlate with perilacunar modulus gradation

Lacunar size and shape change in aging and are commonly studied with a variety of imaging techniques (e.g., CLSM, high-resolution computed tomography). Therefore, it would be useful to understand whether lacunar morphology can be used as an indication of perilacunar bone quality. We evaluated the strength of relationships between lacunar size and measures of modulus gradation (Table S1). The strongest Pearson correlation was lacuna major axis length vs. mean normalized edge:peak modulus, with $r = -0.427$. These results demonstrate that lacunar geometry is overall not a strong indicator of measures related to perilacunar modulus gradation.

### 3.5. Bone tissue hydration impacts some aspects of perilacunar modulus gradation

Because dehydration and embedding stiffen bone tissue [54–56], we sought to estimate the impacts of PMMA-embedding on perilacunar modulus gradation. Six lacunae were mapped at the anterior quadrant of a transverse section of polished, semi-hydrated cortical femur from a 5-month old C57Bl/6 female mouse. Semi-hydrated bone had lower moduli than for PMMA-embedded bone, as expected [57]. An initial rise in modulus from the lacunar wall for the first several hundred nanometers was observed. Modulus versus distance curves normalized to peak values per lacuna demonstrate that the slope of this gradation was similar for PMMA-embedded and semi-hydrated specimens (Figs. S3–4). The peak modulus for semi-hydrated bone is less distinct than for PMMA-embedded bone and occurs at a greater distance from the lacunar

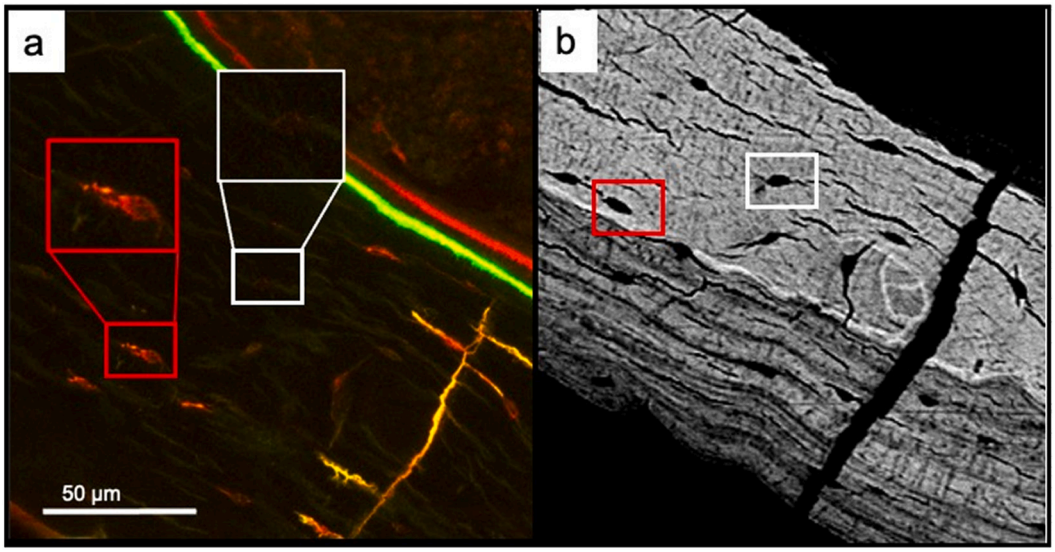


**Fig. 6.** Remodeling osteocytes (red box: alizarin labeled lacuna) versus non-remodeling osteocytes (white box: non-labeled lacuna) imaged with a) confocal laser microscopy (63×-water immersion objective) and b) scanning electron microscopy (carbon coated surface, BSE mode, 15 kV, 400×). The CLSM image is a composite of a Z-stack of images, demonstrating that non-labeled lacunae were not labeled on another slice away from the surface. (For interpretation of the references to colour in this figure legend, the reader is referred to the web version of this article.)

wall (Fig. S4).

## 4. Discussion

The osteocyte lacunar-canalicular system (LCS) is an important contributor to systemic mineral homeostasis. Osteocytes can remove and replace bone mineral around the expansive LCS surface. However, significant questions remain about the impact of LCS remodeling on the quality of bone tissue surrounding this network. Aging truncates LCS morphologies [20,21,26,28,58] and increases the prevalence of osteocyte apoptosis and senescence [25,59–61]. Therefore, we were motivated to investigate whether osteocyte perilacunar bone modulus gradation, one aspect of bone quality, differs between bone-forming and non-bone-forming osteocytes, and to estimate the impact of aging on these characteristics. We utilized confocal laser scanning microscopy and atomic force microscopy to evaluate gradations in perilacunar bone modulus around bone-forming and non-bone forming cortical femur osteocytes for skeletally mature young adult (5-month) and early-old-age (22-month) C57Bl/6 females.

Because synchrotron radiation studies show graded bone mineralization within hundreds of nanometers near lacunar and canalicular surfaces [1,4,49,62–64], our first task was to determine the resolution at which we could resolve gradation in perilacunar moduli. We used AFM to map modulus for 12 μm × 12 μm areas surrounding lacunae (512 × 512 points, ~ 20 nm resolution, ~5 nm indentation depth) and developed an analysis procedure to assess mean modulus at distance increments from the lacunar wall. Using the same maps from an initial set of osteocyte scans from an adult female C57Bl/6 mouse, we investigated modulus gradation from the lacunar wall at 0.2–1 μm step sizes outwards to 2 μm from lacunae (Fig. 3). Our data indicate that at 0.2 μm resolution, an increase in modulus to a peak value is apparent, usually within 0.2–0.4 μm from the lacunar wall. At either 0.5 or 1 μm step size, these peak values are not resolved. However, decrease in bone tissue variability with distance from the lacunar wall was resolved at all three step sizes (Fig. 2b). Importantly, our results indicate that many common microscale-resolution bone quality assessment techniques (e.g., instrumented nanoindentation, Raman spectroscopy, quantitative backscattered SEM) may not have adequate resolution to observe gradation in perilacunar bone quality. This is consistent with prior work, where bone material is often observed to not vary at the microscale surrounding lacunae, outside of circumstances with large perturbations to mineral homeostasis [6,43,45,65–68].

A persistent challenge in osteocyte research is in relating the behavior of individual osteocytes with the impacts to the surrounding bone tissue material. This connection remains elusive, in part because the fixation and decalcification steps necessary to assess parameters of osteocyte behavior (e.g., apoptosis, senescence) generally preclude the determination of bone material properties. In the present work, we introduce a strategy to evaluate the modulus of bone surrounding fluorochrome-labeled or unlabeled osteocyte lacunae. In several prior murine studies, genetic disruptions to LCS bone remodeling decrease the abundance of fluorochrome-labeled cortical lacunae [32,41]. Since these studies decreased osteocyte remodeling and also utilized similar label dosage and timing as our study, we posit that labeled lacunae are likely an indicator of osteocyte bone formation. We also note that the percentage of labeled osteocytes estimated in our study is similar to the percentage of calcein-labeled lacunae (labels administered 2d before euthanasia) measured at the cortical femur for 28d C57Bl/6 mice in previous work by Kegelman and coauthors [41]. Interestingly, labeled lacunae were also abundant in 22-month-old mice in our study, suggesting that LCS remodeling is still quite active at the cortical femur in early-old-age female mice. It is not yet known if perilacunar labeling frequency decreases with more advanced aging.

Our findings demonstrate that lacunae labeled with alizarin administered 2 days before euthanasia have distinct modulus gradations compared with non-labeled lacunae. Specifically, the peak and bulk moduli are lower for labeled lacunae. The RMSE surface roughness was very similar between maps generated for labeled (24.9 ± 5.9 nm) and non-labeled lacunae (23.7 ± 5.2 nm), demonstrating that the differences in perilacunar modulus with labeling are unlikely to be attributed to difference in topography between these groups. Labels extended hundreds of nanometers to ~1 μm in width beyond the lacunar wall (Fig. 7, Fig. S6). It is possible that the labeling itself alters the mineral properties of the bone [69], although it is not determined whether and how this would be expected to influence the bone modulus. Perilacunar modulus gradations were only moderately correlated with lacunar geometry. Thus, morphological techniques alone are not sufficient for assessing changes to perilacunar bone modulus.

The gradations in PMMA-embedded bone are in excellent agreement with synchrotron studies that studied gradation in mineral near the LCS

**Table 1**
Measurements of lacunar morphological and modulus properties for 5-month and 22-month old mice for bone-forming and non-bone-forming lacunae: Data are presented as marginal mean (adjusted for age and label) ± standard error from mixed-model ANOVA. Non-significant *p*-values are noted for $p \leq 0.10$.

| Measures | 5-months | | 22-months | |
|---|---|---|---|---|
| | Non-labeled n = 5 mice 5 lacunae / mouse | Labeled $n = 5$ mice 5 lacunae / mouse | Non-labeled n = 5 mice 5 lacunae / mouse | Labeled n = 5 mice 5 lacunae / mouse |
| Lacuna cross-sectional area ($\mu m^2$)<br>Age: NS<br>Label: NS<br>Age x Label: NS | 15.18 ± 1.38 | 16.05 ± 1.20 | 14.27 ± 1.40 | 13.10 ± 1.21 |
| Lacuna major axis length (μm)<br>Age: $p = 0.032$<br>Label: NS<br>Age x Label: NS | 10.31 ± 0.53 | 10.62 ± 0.43 | 9.13 ± 0.53 | 9.30 ± 0.43 |
| Lacuna minor axis length (μm)<br>Age: NS<br>Label: NS<br>Age x Label: NS | 3.72 ± 0.24 | 3.95 ± 0.19 | 4.07 ± 0.24 | 3.55 ± 0.19 |
| Lacuna sphericity<br>Age: $p = 0.081$<br>Label: NS<br>Age x Label: $p = 0.092$ | 0.361 ± 0.028 | 0.385 ± 0.023 | 0.452 ± 0.028 | 0.386 ± 0.023 |
| Peak mean modulus (GPa)<br>Age: NS<br>Label: $p = 0.014$<br>Age x Label: NS | 38.20 ± 3.38 | 32.78 ± 3.23 | 31.39 ± 3.40 | 28.66 ± 3.24 |
| Area before peak mean modulus (data inversely transformed, $\mu m^{-2}$)<br>Age: NS<br>Label: NS<br>Age x Label: NS | 0.115 ± 0.013 | 0.094 ± 0.011 | 0.105 ± 0.013 | 0.100 ± 0.011 |
| Bulk mean modulus (GPa)<br>Age: NS<br>Label: $p = 0.031$<br>Age x Label: NS | 34.04 ± 3.19 | 30.21 ± 3.07 | 28.80 ± 3.21 | 26.30 ± 3.08 |
| Area before peak standard deviation of modulus (data inversely transformed, $\mu m^{-2}$)<br>Age: NS<br>Label: NS<br>Age x Label: NS | 0.230 ± 0.023 | 0.214 ± 0.019 | 0.248 ± 0.023 | 0.0228 ± 0.019 |
| Δ Modulus (peak-bulk) (GPa)<br>Age: NS<br>Label: $p = 0.10$<br>Age x Label: NS | 4.06 ± 0.63 | 2.65 ± 0.54 | 2.68 ± 0.64 | 2.30 ± 0.55 |
| Normalized modulus bulk: peak<br>Age: NS<br>Label: $p = 0.08$<br>Age x Label: NS | 0.88 ± 0.02 | 0.92 ± 0.01 | 0.91 ± 0.02 | 0.92 ± 0.01 |
| Modulus slope, peak to bulk (GPa/μm)<br>Age: $p = 0.036$<br>Label: NS<br>Age x Label: NS | −2.54 ± 0.36 | −2.22 ± 0.30 | −1.82 ± 0.36 | −1.52 ± 0.30 |
| Normalized modulus edge: peak<br>Age: NS<br>Label: NS<br>Age x Label: NS | 0.68 ± 0.03 | 0.72 ± 0.03 | 0.75 ± 0.03 | 0.73 ± 0.03 |
| Modulus slope, edge to peak (GPa/μm)<br>Age: 0.070<br>Label: NS<br>Age x Label: NS | 50.55 ± 6.97 | 34.01 ± 6.00 | 25.94 ± 7.06 | 28.16 ± 6.05 |
| Peak standard deviation of modulus (GPa)<br>Age: NS<br>Label: $p = 0.032$<br>Age x Label: NS | 14.68 ± 1.46 | 12.27 ± 1.40 | 11.40 ± 1.47 | 10.93 ± 1.41 |
| Bulk standard deviation of modulus (GPa)<br>Age: NS<br>Label: $p = 0.010$<br>Age x Label: NS | 10.42 ± 1.06 | 9.00 ± 1.02 | 8.49 ± 1.06 | 7.53 ± 1.02 |
| Δ Standard deviation of modulus (peak-bulk) (GPa)<br>Age: NS<br>Label: NS<br>Age x Label: $p = 0.070$ | 4.26 ± 0.90 | 3.27 ± 0.85 | 2.90 ± 0.91 | 3.41 ± 0.86 |
| Normalized standard deviation of modulus, bulk:peak<br>Age: NS<br>Label: NS<br>Age x Label: $p = 0.014$ | 0.67 ± 0.05 | 0.76 ± 0.04 | 0.77 ± 0.05 | 0.70 ± 0.04 |
| Standard deviation of modulus slope, peak to bulk (GPa/μm)<br>Age: NS<br>Label: NS<br>Age x Label: NS | −2.39 ± 0.49 | −1.82 ± 0.46 | −1.61 ± 0.49 | −2.02 ± 0.46 |

in dehydrated human [49] and dehydrated ovine bone [70]. Hesse and co-authors studied lacunae and canaliculi from human mandible and found that mass density increased from the LCS walls to a peak at about 0.2 μm. These peak values were followed by a decrease in mass density with further distance from the LCS walls [49]. In another study, Nango and colleagues assessed lacunae and canaliculi for wild-type and osteoporotic mice using a combination of synchrotron x-ray microscopy and transmission electron microscopy (TEM). The lowest mineralization was adjacent to the lacunar wall and increased with distance to either a peak or an asymptotic value [1]. The close correspondence between our AFM modulus profiles from PMMA-embedded bone and variation in mass or mineral density at a similar length-scale suggests that our observed modulus gradation reflects variation in bone mineral.

Bone dehydration and embedding increase bone modulus [54–56]. Thus, we sought to estimate the impact of bone dehydration on bone modulus gradation. We completed a preliminary assessment of bone modulus gradation in semi-hydrated bone for six lacunae from the femur of one 5-month old C57Bl/6 female that had not been mechanically tested. The sample was considered semi-hydrated because the hydrated bone surface was wicked dry to avoid hydrodynamic interactions between the cantilever and a fluid layer. As expected, semi-hydrated bone tissue has lower modulus than PMMA-embedded bone. When normalized to the peak value per lacunae, it is apparent that the initial steep gradation in the first 400 nm from the lacunar wall is similar for semi-hydrated and PMMA-embedded samples (Fig. S4). The PMMA-embedded samples show a clear peak modulus value after the initial rise in modulus and then a distinct taper to a bulk modulus value (Fig. S4). By contrast, semi-hydrated bone does not produce a peak value after the initial rise in modulus. The differences in modulus profiles may relate to the decreased sensitivity of dehydrated bone modulus to properties of the organic matrix, such as collagen fibril orientation [55]. Mineral gradations near the lacunar edge in semi-hydrated bone appear to correspond to a dominant effect of change in mineralization on

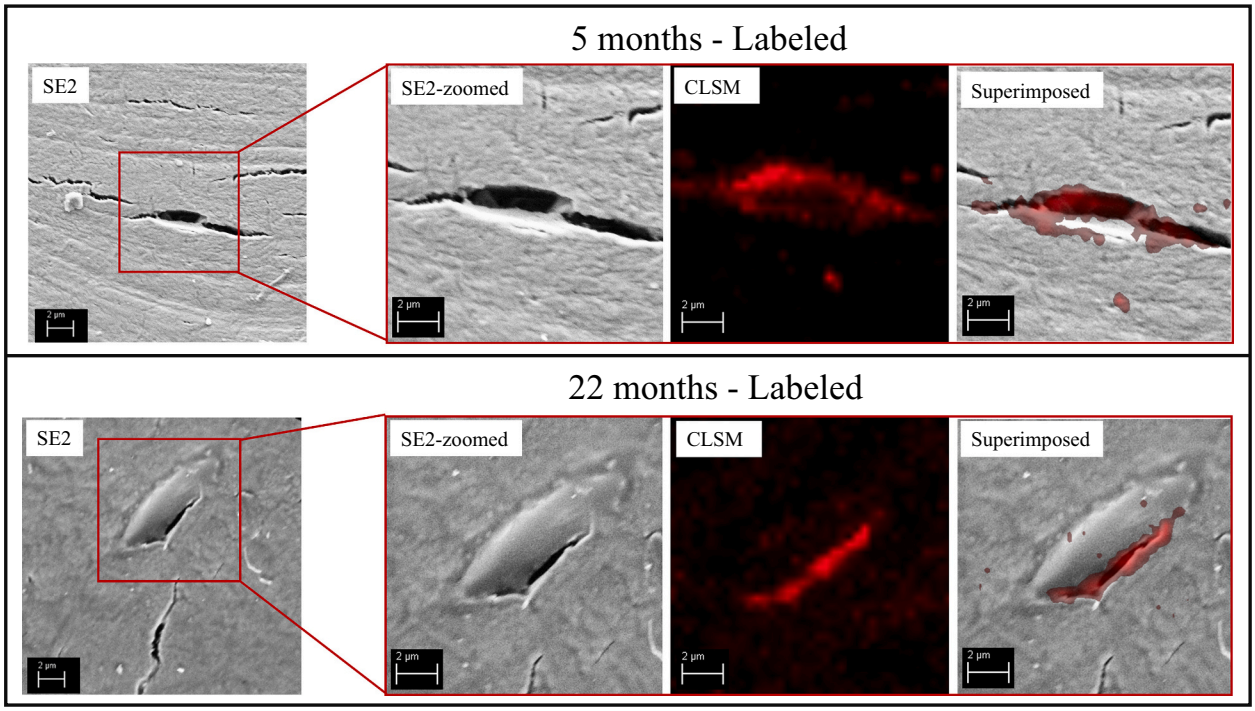


**Fig. 7.** Superimposition of CLSM images with secondary mode images from FESEM. The FESEM images were collected at 8-10kx, 4 kV, 9.1 mm working distance).

modulus, since these gradations are in good agreement with PMMA-embedded bone. However, in the more mineralized bone farther from the lacunar wall, this variation in modulus is more likely to reflect variation in the properties and structure of the hydrated organic matrix. Thus, we posit that the relatively larger contribution of the organic matrix to the modulus in semi-hydrated bone may influence the location and value of the peak modulus. The purpose of the semi-hydrated versus PMMA-embedded bone comparison was to estimate the effects of hydration on bone modulus gradation. A more extensive investigation would be required to interpret differences in the effects of labeling and aging on hydrated bone.

Perilacunar bone modulus gradation may be influenced by a combination of active and passive mineralization and demineralization processes. Some degree of passive mineral exchange may occur, since modulus is still graded, albeit differently, for unlabeled lacunae. Mineral exchange could be influenced by direct calcium exchange between bone local to the LCS and interstitial fluid [49]. As suggested by Hesse and co-authors, mass density gradients followed by a peak may indicate a diffusion limit for calcium ions from LCS into the extracellular matrix (ECM). The authors used the size of this zone of lower mass density to estimate the availability of rapidly-exchangeable calcium [49]. However, our finding that labeled lacunae have distinct modulus gradations suggests that mineralization and demineralization processes may have an active contribution from the living osteocyte. Furthermore, osteocytes from human mandible specimens with bisphosphonate-induced necrosis, which are more likely to be apoptotic, also had distinct perilacunar and pericanalicular mass gradation compared with healthy comparisons [49]. Thus, it is possible that contributions from active and passive mineralization and demineralization processes change in diseases and physiological processes where osteocyte viability declines, but addressing these questions requires further investigation.

Aging affected some characteristics of perilacunar modulus gradation and lacunar size in this study, but we were likely underpowered to detect the effect on age on several other measures given our small sample size ($n = 5$ mice/age). Age significantly decreased the modulus slope from peak to bulk. On the other hand, the modulus slope from edge to peak was lower for aged mice but the comparison was not significant ($p = 0.081$). Likewise, there was a significant difference in lacunar major axis length with aging, but we did not observe significant differences for other measures of lacunar size and shape that may be expected to change in aging. In particular, lacunar sphericity is expected to increase with aging, but the comparison between young adult and early-old-age mice was not significant in this study ($p = 0.070$). Overall, the specific impacts of perilacunar remodeling on lacunar shape and perilacunar modulus gradation would benefit from investigating more mice across an extended age range.

There are several potential reasons why perilacunar bone modulus gradation may have consequences to the osteocyte. The average perilacunar bone area before the peak modulus for labeled lacunae was 16 $\mu m^2$ for PMMA-embedded bone. Because osteocyte lacunae are abundantly labeled, we can estimate that a sizable surface of bone along the expansive LCS has lower modulus associated with osteocyte bone formation. Therefore, changes to osteocyte remodeling with advanced aging or disease may be a mechanism by which bone mineral and matrix are modified. However, while it is possible that the changes seen in perilacunar tissue modulus may affect whole-bone mechanical properties, further studies would be necessary to directly link bone quality across these length-scales. Perilacunar modulus gradation may have a physical consequence to the osteocyte. For instance, a softer zone around the lacuna would be expected to increase the strain experienced by the osteocyte [46,71,72]. Prior computational estimates of osteocyte strain amplification based on differences between perilacunar and bulk bone properties assigned 10 μm of perilacunar tissue with different moduli based on a parametric analysis [71,72]. Another study used instrumented nanoindentation to estimate perilacunar properties for the first 5 μm from lacunar walls to use as finite element model inputs [46]. The findings from our present work as well as the methods we share for analyzing 2D AFM modulus maps could be utilized to improve estimates about the effect of perilacunar modulus gradation on osteocyte strain amplification in the contexts of bone-forming and non-bone forming osteocytes.

Our study has several limitations. First, bone samples were dehydrated in ethanol and embedded in PMMA. We compared our perilacunar modulus gradation from PMMA-embedded bone with bones that

were not embedded and were instead hydrated with tap water. Semi-hydrated bone samples still showed perilacunar modulus gradation, but these gradations had several differences from the PMMA-embedded samples. Next, we did not identify the cause of the bone modulus gradation. It would be valuable to ascertain bone compositional differences at similar length-scales to those probed with AFM, although this is technically quite challenging. Another limitation is that pericanalicular bone tissue was not mapped in this study. In synchrotron studies, bone mass gradation around canaliculi is similar to around lacunae [49], suggesting that AFM may also resolve modulus gradation around these structures. The approach presented herein could be readily modified to map modulus around canaliculi or dendrites. We did not evaluate whether aging decreases the number or proportion of labeled lacunae. However, of all the randomly selected lacunae in this study, a similar proportion was labeled for young adult and early-old-age mice. Finally, this study assessed a small number ($n = 5$ / group) of young adult and early-old-age C57Bl/6 female mice. While we observed modulus gradation for every perilacunar bone map acquired for both ages, the causes of changes of modulus profiles with age would benefit from additional mice of both sexes across an extended age range.

## 5. Conclusions

We report, for the first time, that bone modulus is graded at the sub-micrometer scale around osteocyte lacunae. Perilacunar modulus gradation is distinct for fluorochrome-labeled lacunae for both skeletally-mature young adult and early-old age mice, where the labeled lacunae are surrounded by a region of lower modulus bone. However, perilacunar modulus gradation is not strongly related to the 2D dimensions of the lacuna. Given the immense scale of the LCS and the abundance of osteocyte bone formation, our findings support the possibility that lacunar-canalicular remodeling can impact bone tissue properties, such as modulus.

## Abbreviations

| | |
|---|---|
| LCS | lacunar-canalicular system |
| AFM | atomic force microscopy |
| CLSM | confocal laser scanning microscopy |

## CRediT authorship contribution statement

Caleb J. Rux: Investigation, software, formal analysis, data curation, visualization, writing – original draft, writing – review & editing.

Ghazal Vahidi: Investigation, visualization, writing – review & editing.

Amir Darabi: Investigation, writing – review & editing.

Lewis M. Cox: Methodology, resources, data curation, writing – review & editing.

Chelsea M. Heveran: Conceptualization, methodology, formal analysis, data curation, project administration, funding acquisition, data curation, writing – original draft, writing – review & editing.

## Data availability

MATLAB code data have been deposited in the GitHub repository: https://github.com/cjrux/Osteocyte_Boundary_Analysis

## Acknowledgements

This work was supported by NIH R03 AG068680, NSF CMMI-2120239, and NIH P20 GM103474. This work was performed in part at the Montana Nanotechnology Facility, a member of the National Nanotechnology Coordinated Infrastructure (NNCI), which is supported by the National Science Foundation (Grant# ECCS-2025391). We thank Dr. Heidi Smith at the Montana State University Center for Biofilm Engineering for assistance with CLSM imaging.

## Appendix A. Supplementary data

Supplementary data to this article can be found online at https://doi.org/10.1016/j.bone.2022.116327.

## References

[1] N. Nango, S. Kubota, T. Hasegawa, W. Yashiro, A. Momose, K. Matsuo, Osteocyte-directed bone demineralization along canaliculi, Bone 84 (2016) 279–288.
[2] S. Okada, S. Yoshida, S.H. Ashrafi, D.E. Schraufnagel, The canalicular structure of compact bone in the rat at different ages, Microsc. Microanal. 8 (2) (2002) 104–115.
[3] R. Weinkamer, P. Kollmannsberger, P. Fratzl, Towards a connectomic description of the osteocyte lacunocanalicular network in bone, Curr. Osteoporos. Rep. 17 (4) (2019) 186–194.
[4] F. Peyrin, P. Dong, A. Pacureanu, M. Langer, Micro- and nano-CT for the study of bone ultrastructure, Curr. Osteoporos. Rep. 12 (4) (2014) 465–474.
[5] L.F. Bonewald, The amazing osteocyte, J. Bone Miner. Res. 26 (2) (2011) 229–238.
[6] S. Zhang, F.L. Bach-gansmo, D. Xia, F. Besenbacher, H. Birkedal, Nanostructure and Mechanical Property of the Osteocyte Lacunar-Canalicular Network Associated Bone Matrix Revealed by Quantitative Nanomechanical Mapping, 2015.
[7] P.R. Buenzli, N.A. Sims, Quantifying the osteocyte network in the human skeleton, Bone 75 (2015) 144–150.
[8] S.L. Dallas, M. Prideaux, L.F. Bonewald, The osteocyte: an endocrine cell and more, Endocr. Rev. 34 (5) (2013) 658–690.
[9] A.G. Robling, L.F. Bonewald, The osteocyte: new insights, Annu. Rev. Physiol. 82 (2020) 485–506.
[10] L.F. Belanger, B. Migicovsky, Histochemical evidence of proteolysis in bone: the influence of parathormone, J. Histochem. Cytochem. 11 (6) (1963) 734–737.
[11] H. Qing, L. Ardeshirpour, P. Divieti Pajevic, V. Dusevich, K. Jähn, S. Kato, J. Wysolmerski, L.F. Bonewald, Demonstration of osteocytic perilacunar/canalicular remodeling in mice during lactation, J. Bone Miner. Res. 27 (5) (2012) 1018–1029.
[12] J.J. Wysolmerski, Osteocytic osteolysis: time for a second look? Bonekey Rep. 1 (October) (2012) 229.
[13] K. Tazawa, K. Hoshi, S. Kawamoto, M. Tanaka, S. Ejiri, H. Ozawa, Osteocytic osteolysis observed in rats to which parathyroid hormone was continuously administered, JBMR 22 (2004) 524–529.
[14] L.F. Bélanger, Osteocytic osteolysis, Calcif. Tissue Res. 4 (1) (1969) 1–12.
[15] S. Kaya, J. Basta-Pljakic, Z. Seref-Ferlengez, R.J. Majeska, L. Cardoso, T. G. Bromage, Q. Zhang, C.R. Flach, R. Mendelsohn, S. Yakar, S.P. Fritton, M. B. Schaffler, Lactation-induced changes in the volume of osteocyte lacunar-canalicular space alter mechanical properties in cortical bone tissue, J. Bone Miner. Res. 32 (4) (2017) 688–697.
[16] A. Yajima, K. Tsuchiya, D.B. Burr, D.E. Minner, K.W. Condon, C.A. Miller, S. Satoh, M. Inaba, T. Nakayama, T. Tanizawa, A. Ito, K. Nitta, Osteocytic perilacunar/canalicular turnover in hemodialysis patients with high and low serum PTH levels, Bone 113 (May) (2018) 68–76.
[17] A. Sekita, A. Matsugaki, T. Ishimoto, T. Nakano, Synchronous disruption of anisotropic arrangement of the osteocyte network and Collagen/Apatite in melanoma bone metastasis, J. Struct. Biol. 197 (3) (2017) 260–270.
[18] J.M. Swift, S.N. Swift, M.R. Allen, S.A. Bloomfield, in: Beta-1 Adrenergic Agonist Treatment Mitigates Negative Changes in Cancellous Bone Microarchitecture and Inhibits Osteocyte Apoptosis During Disuse 9, 2014, pp. 1–8 (9).
[19] M. Gerbaix, V. Gnyubkin, D. Farlay, C. Olivier, P. Ammann, G. Courbon, N. Laroche, R. Genthial, H. Follet, F. Peyrin, B. Shenkman, G. Gauquelin-koch, L. Vico, One-month spaceflight compromises the bone mechanical properties, osteocyte survival and lacunae volume in mature mice skeletons, Sci. Rep. 7 (1) (2017) 2659.
[20] L.M. Tiede-Lewis, M.A. Hulbert, R. Campos, M.R. Dallas, L.F. Bonewald, S. L. Dallas, Degeneration of the osteocyte network in the C57Bl/6 mouse model of aging, Aging (Albany. NY) 9 (10) (2017) 2190–2208.
[21] C.M. Heveran, A. Rauff, K.B. King, R.D. Carpenter, V.L. Ferguson, A new open-source tool for measuring 3D osteocyte lacunar geometries from confocal laser scanning microscopy reveals age-related changes to lacunar size and shape in cortical mouse bone, Bone 110 (2018).
[22] C.S. Kovacs, The skeleton is a storehouse of mineral that is plundered during lactation and (fully?) replenished afterwards, J. Bone Miner. Res. 32 (4) (2017) 676–680.
[23] C.A. Schurman, S.W. Verbruggen, T. Alliston, Disrupted osteocyte connectivity and pericellular fluid flow in bone with aging and defective TGF-β signaling, Proc. Natl. Acad. Sci. U. S. A. 118 (25) (2021) 1–11.
[24] A.M. Ashique, L.S. Hart, C.D.L. Thomas, J.G. Clement, P. Pivonka, Y. Carter, D. D. Mousseau, D.M.L. Cooper, Lacunar-Canalicular Network in Femoral Cortical Bone Is Reduced in Aged Women and Is Predominantly Due to a Loss of Canalicular Porosity, 2017.
[25] F.L. Bach-Gansmo, A. Brüel, M.V. Jensen, E.N. Ebbesen, H. Birkedal, J.S. Thomsen, Osteocyte lacunar properties and cortical microstructure in human iliac crest as a function of age and sex, Bone 91 (2016) 11–19.
[26] C.M. Heveran, C. Schurman, C. Acevedo, E.W. Livingston, D. Howe, E.G. Schaible, H. Hunt, A. Rauff, E. Donnelly, R.D. Carpenter, M. Levi, A. Lau, T. Bateman,

T. Alliston, K.B. King, V.L. Ferguson, Chronic kidney disease and aging differentially diminish bone material and microarchitecture in C57Bl/6 mice, Bone 127 (April) (2019) 91–103.
[27] L.A.M. Tiede-Lewis, S.L. Dallas, Changes in the osteocyte lacunocanalicular network with aging, Bone 122 (February) (2019) 101–113.
[28] Y. Carter, C. David, L. Thomas, J.G. Clement, D.M.L. Cooper, Femoral osteocyte lacunar density, volume and morphology in women across the lifespan, J. Struct. Biol. 183 (3) (2013) 519–526.
[29] H. Hemmatian, A.D. Bakker, J. Klein-Nulend, G.H. van Lenthe, Aging, osteocytes, and mechanotransduction, Curr. Osteoporos. Rep. 15 (5) (2017) 401–411.
[30] R.L. Jilka, C.A. O'Brien, The role of osteocytes in age-related bone loss, Curr. Osteoporos. Rep. 14 (1) (2016) 16–25.
[31] N.S. Dole, C.M. Mazur, C. Acevedo, R.O. Ritchie, K.S. Mohammad, T. Alliston, N. S. Dole, C.M. Mazur, C. Acevedo, J.P. Lopez, D.A. Monteiro, T.W. Fowler, R. O. Ritchie, K.S. Mohammad, T. Alliston, Osteocyte-intrinsic TGF- b signaling regulates bone article osteocyte-intrinsic TGF- b signaling regulates bone quality through perilacunar / canalicular remodeling, Cell Rep. 21 (9) (2017) 2585–2596.
[32] S.Y. Tang, R.P. Herber, S.P. Ho, T. Alliston, Matrix metalloproteinase-13 is required for osteocytic perilacunar remodeling and maintains bone fracture resistance, J. Bone Miner. Res. 27 (9) (2012) 1936–1950.
[33] E.A. Zimmermann, R.O. Ritchie, Bone as a structural material, Adv. Healthc. Mater. 4 (9) (2015) 1287–1304.
[34] G. Vahidi, C. Rux, V.D. Sherk, C.M. Heveran, Lacunar-canalicular bone remodeling: impacts on bone quality and tools for assessment, Bone 143 (2021), 115663.
[35] K. Wang, Y. Ren, S. Lin, Y. Jing, C. Ma, J. Wang, X.B. Yuan, X. Han, H. Zhao, Z. Wang, M. Zheng, Y. Xiao, L. Chen, B.R. Olsen, J.Q. Feng, Osteocytes but not osteoblasts directly build mineralized bone structures, Int. J. Biol. Sci. 17 (10) (2021) 2430–2448.
[36] S.M. van Gaalen, M.C. Kruyt, R.E. Geuze, J.D. de Bruijn, J. Alblas, W.J.A. Dhert, Use of fluorochrome labels in in vivo bone tissue engineering research, Tissue Eng. Part B 16 (2) (2010) 209–217.
[37] C. Pautke, S. Vogt, T. Tischer, G. Wexel, H. Deppe, S. Milz, M. Schieker, A. Kolk, Polychrome labeling of bone with seven different fluorochromes: enhancing fluorochrome discrimination by spectral image analysis, Bone 37 (4) (2005) 441–445.
[38] T. Calderón, W. Arnold, G. Stalder, J. Painer, M. Köhler, Labelling experiments in Red Deer provide a general model for early bone growth dynamics in ruminants, Sci. Rep. 11 (1) (2021) 1–14.
[39] B.A. Rahn, S.M. Perren, Xylenol Orange, a fluorochrome useful in polychrome sequential labeling of calcifying tissues, Biotech. Histochem. 46 (3) (1971) 125–129.
[40] A. Carriero, A.F. Pereira, A.J. Wilson, S. Castagno, B. Javaheri, A.A. Pitsillides, M. Marenzana, S.J. Shefelbine, Spatial relationship between bone formation and mechanical stimulus within cortical bone: combining 3D fluorochrome mapping and poroelastic finite element modelling, Bone Rep. 8 (February) (2018) 72–80.
[41] C.D. Kegelman, J.C. Coulombe, K.M. Jordan, D.J. Horan, L. Qin, A.G. Robling, V. L. Ferguson, T.M. Bellido, J.D. Boerckel, YAP and TAZ mediate osteocyte Perilacunar/Canalicular remodeling, J. Bone Miner. Res. 35 (1) (2020) 196–210.
[42] D.J. Baylink, J.E. Wergedal, Bone formation by osteocytes, Am. J. Phys. 221 (3) (1971) 669–678.
[43] N.E. Lane, W. Yao, M. Balooch, R.K. Nalla, G. Balooch, S. Habelitz, J.H. Kinney, L. F. Bonewald, Glucocorticoid-treated mice have localized changes in trabecular bone material properties and osteocyte lacunar size that are not observed in placebo-treated or estrogen-deficient mice, J. Bone Miner. Res. 21 (3) (2005) 466–476.
[44] J.D. Gardinier, S. Al-Omaishi, M.D. Morris, D.H. Kohn, PTH signaling mediates perilacunar remodeling during exercise, Matrix Biol. 52–54 (2016) 162–175.
[45] D. Sharma, C. Ciani, P.A.R. Marin, J.D. Levy, S.B. Doty, S.P. Fritton, Alterations in the osteocyte lacunar-canalicular microenvironment due to estrogen deficiency, Bone 51 (3) (2012) 488–497.
[46] A.R. Stern, X. Yao, Y. Wang, A. Berhe, M. Dallas, M.L. Johnson, W. Yao, D. B. Kimmel, N.E. Lane, Effect of osteoporosis treatment agents on the cortical bone osteocyte microenvironment in adult estrogen-deficient, osteopenic rats, Bone Rep. 8 (January) (2018) 115–124.
[47] P. Milovanovic, E.A. Zimmermann, M. Hahn, D. Djonic, K. Püschel, M. Djuric, M. Amling, B. Busse, Osteocytic canalicular networks: morphological implications for altered mechanosensitivity, ACS Nano 7 (9) (2013) 7542–7551.
[48] F.L. Bach-Gansmo, J.C. Weaver, M.H. Jensen, H. Leemreize, K.S. Mader, M. Stampanoni, A. Brüel, J.S. Thomsen, H. Birkedal, Osteocyte lacunar properties in rat cortical bone: differences between lamellar and central bone, J. Struct. Biol. 191 (1) (2015) 59–67.
[49] B. Hesse, P. Varga, M. Langer, A. Pacureanu, S. Schrof, N. Männicke, H. Suhonen, P. Maurer, P. Cloetens, F. Peyrin, K. Raum, Canalicular network morphology is the major determinant of the spatial distribution of mass density in human bone tissue: evidence by means of synchrotron radiation phase-contrast Nano-CT, J. Bone Miner. Res. 30 (2) (2015) 346–356.
[50] V.H.H. Hertz, in: Die Lieber Die Berührung Fester Elastischer Körper, 1878, pp. 156–171.
[51] J.P. Killgore, R.H. Geiss, D.C. Hurley, Continuous measurement of atomic force microscope tip wear by contact resonance force microscopy, Small 7 (8) (2011) 1018–1022.
[52] K.H. Chung, Y.H. Lee, D.E. Kim, Characteristics of fracture during the approach process and wear mechanism of a silicon AFM tip, Ultramicroscopy 102 (2) (2005) 161–171.
[53] S. Kim, R. Casper, in: Applications of Convolution in Image Processing with MATLAB, Univ. Washingt., 2013, pp. 1–20.
[54] A. Bushby, V. Ferguson, A. Boyde, Nanoindentation of bone: comparison of specimens tested in liquid and embedded in polymethylmethacrylate, J. Mater. Res. 19 (01) (2004) 249–259.
[55] L. Feng, M. Chittenden, J. Schirer, M. Dickinson, I. Jasiuk, Mechanical properties of porcine femoral cortical bone measured by nanoindentation, J. Biomech. 45 (10) (2012) 1775–1782.
[56] M. Granke, M.D. Does, J.S. Nyman, The role of water compartments in the material properties of cortical bone, Calcif. Tissue Int. 97 (2015) 292–307.
[57] V.L. Ferguson, A.J. Bushby, A. Boyde, Nanonmechanical properties and mineral concentration in articular calcified cartilage and subchondral bone, J. Anat. 203 (2) (2003) 191–202.
[58] H. Hemmatian, M.R. Laurent, A.D. Bakker, D. Vanderschueren, J. Klein-Nulend, G. H. van Lenthe, Age-related changes in female mouse cortical bone microporosity, Bone 113 (April) (2018) 1–8.
[59] B. Busse, D. Djonic, P. Milovanovic, M. Hahn, K. Püschel, R.O. Ritchie, M. Djuric, M. Amling, Decrease in the osteocyte lacunar density accompanied by hypermineralized lacunar occlusion reveals failure and delay of remodeling in aged human bone, Aging Cell 9 (6) (2010) 1065–1075.
[60] D. Vashishth, O. Verborgt, G. Divine, M.B. Schaffler, D.P. Fyhrie, Decline in osteocyte lacunar density in human cortical bone is associated with accumulation of microcracks with age, Bone 26 (4) (2000) 375–380.
[61] M.G. Mullender, D.D. Van Der Meer, R. Huiskes, P. Lips, Osteocyte density changes in aging and osteoporosis, Bone 18 (2) (1996) 109–113.
[62] S.I. Djomehri, S. Candell, T. Case, A. Browning, G.W. Marshall, W. Yun, S.H. Lau, S. Webb, S.P. Ho, Mineral density volume gradients in normal and diseased human tissues, PLoS One 10 (4) (2015), e0121611.
[63] G.J. Kazakia, A.J. Burghardt, S. Cheung, S. Majumdar, Assessment of bone tissue mineralization by conventional X-ray microcomputed tomography: comparison with synchrotron radiation microcomputed tomography and ash measurements, Med. Phys. 35 (7Part1) (2008) 3170–3179.
[64] S. Nuzzo, M.H. Lafage-Proust, E. Martin-Badosa, G. Boivin, T. Thomas, C. Alexandre, F. Peyrin, Synchrotron radiation microtomography allows the analysis of three-dimensional microarchitecture and degree of mineralization of human iliac crest biopsy specimens: effects of etidronate treatment, J. Bone Miner. Res. 17 (8) (2002) 1372–1382.
[65] J.D. Gardinier, S. Al-Omaishi, N. Rostami, M.D. Morris, D.H. Kohn, Examining the influence of PTH(1–34) on tissue strength and composition, Bone 117 (September) (2018) 130–137.
[66] E.A. Taylor, E. Donnelly, X. Yao, M.L. Johnson, S.K. Amugongo, D.B. Kimmel, N. E. Lane, Sequential treatment of estrogen deficient, osteopenic rats with alendronate, parathyroid hormone (1–34), or raloxifene alters cortical bone mineral and matrix composition, Calcif. Tissue Int. 106 (3) (2020) 303–314.
[67] G. Mabilleau, R. Perrot, P.R. Flatt, N. Irwin, D. Chappard, High fat-fed diabetic mice present with profound alterations of the osteocyte network, Bone 90 (2016) 99–106.
[68] S. Kaya, J. Basta-Pljakic, Z. Seref-Ferlengez, R. Majeska, L. Cardoso, T. Bromage, Q. Zhang, C.R. Flach, R. Mendelsohn, S. Yakar, S.P. Fritton, M.B. Shaffler, Lactation-induced changes in the volume of osteocyte lacunar-canalicular space alter mechanical properties in cortical bone tissue, J. Bone Miner. Res. 32 (4) (2017) 688–697.
[69] M. Aido, M. Kerschnitzki, R. Hoerth, M. Burghammer, C. Montero, S. Checa, P. Fratzl, G.N. Duda, B.M. Willie, M. Aido, M. Kerschnitzki, R. Hoerth, M. Burghammer, C. Montero, S. Checa, P. Fratzl, G.N. Duda, B.M. Willie, P. Fratzl, G.N. Duda, B.M. Willie, W. Wagermaier, Relationship between nanoscale mineral properties and calcein labeling in mineralizing bone surfaces in mineralizing bone surfaces, Connect. Tissue Res. 55 (S1) (2014) 15–17.
[70] M. Kerschnitzki, P. Kollmannsberger, M. Burghammer, G.N. Duda, R. Weinkamer, W. Wagermaier, P. Fratzl, Architecture of the osteocyte network correlates with bone material quality, J. Bone Miner. Res. 28 (8) (2013) 1837–1845.
[71] A.R. Bonivtch, L.F. Bonewald, D.P. Nicolella, Tissue strain amplification at the osteocyte lacuna: a microstructural finite element analysis, J. Biomech. 40 (2007) 2199–2206.
[72] S.K. Kola, M.T. Begonia, L.A.M. Tiede-Lewis, L.E. Laughrey, S.L. Dallas, M. L. Johnson, T. Ganesh, Osteocyte lacunar strain determination using multiscale finite element analysis, Bone Rep. 12 (May) (2020), 100277.